

Research article

Energy Absorption Capacity of Concrete-Filled Steel Tube Slender Columns with Different Aspect Ratios

Alireza Bahrami^{1,2*} and Ali Mahmoudi Kouhi²

¹Department of Building Engineering, Energy Systems, and Sustainability Science, Faculty of Engineering and Sustainable Development, University of Gävle, Gävle, Sweden

²Department of Civil Engineering, Abadan Branch, Islamic Azad University, Abadan, Iran

Received: 27 September 2020, Revised: 26 April 2021, Accepted: 19 May 2021

DOI: 10.55003/cast.2022.01.22.005

Abstract

Keywords

energy absorption capacity;
concrete-filled steel tube slender column;
aspect ratio;
nonlinear analysis;
finite element simulation

The present paper examines the energy absorption capacity of concrete-filled steel tube slender (CFTS) columns having different aspect ratios. The CFTS columns are nonlinearly analysed employing the finite element software ABAQUS. In order to validate the simulation of the columns, an experimentally tested CFTS column is simulated and its achieved result is compared with that of the tested column. Since it is concluded that there is a good agreement between the obtained results from the simulation and experimental test, the validation of the simulation is then established. The simulated columns are thereafter developed using different aspect ratios of 6, 10, and 13 and also considering the following parameters: load eccentricities, cross-sectional shapes, and steel tube thicknesses. The columns are nonlinearly analysed and the results are achieved from the analyses. The effects of the above-mentioned parameters on the energy absorption capacity of the CFTS columns are evaluated. From the results, it can be concluded that the energy absorption capacity of the columns is decreased by the increase of the load eccentricity or aspect ratio. Further, the energy absorption capacity of the circular CFTS column is greater than that of the rectangular and square CFTS columns. However, higher energy absorption capacity is accomplished for the rectangular column than the square column. Additionally, increasing the steel tube thickness leads to greater energy absorption capacity of the columns. Typical failure modes of the columns are assessed.

*Corresponding author: E-mail: Alireza.Bahrami@hig.se

1. Introduction

Concrete-filled steel tube slender (CFTS) columns have widely been garnering attention of structural researchers and practitioners as high-performance structural members. Their achieved great strength, large ductility, and high stiffness have led to their increasing usage in high rise buildings. The CFTS columns are composed of a concrete core confined by the surrounding steel tube. Compressive forces are mainly resisted by the concrete core. Also, the concrete core prevents the inward buckling of the steel tube. On the other hand, the steel tube prevents spalling of the concrete core. Moreover, longitudinal and transverse reinforcements are not required owing to the existence of the steel tube. The steel tube acts as permanent formwork for the concrete core which finally leads to cost saving in terms of the materials and manpower.

The performance of the CFTS columns has been investigated in numerous studies so far. Strength and ductility of concrete-filled steel box columns were assessed under the effects of different materials and geometric properties by Uy [1]. Han and Yao [2] reported the load-deformation behaviour of concrete-filled hollow structural steel columns with steel tubes subjected to preload. Effects of cross-section geometry and concrete strength on the behaviour of concrete-filled cold-formed stainless steel tube columns were evaluated by Ellobody and Young [3]. Stainless steel concrete-filled columns with various concrete compressive strengths were tested by Lam and Gardner [4]. Yang and Han [5] conducted tests of rectangular concrete-filled steel tubular columns under axial loads on a partially stressed cross-sectional area. Starossek *et al.* [6] investigated the force transfer by natural bond or by mechanical shear connectors and the interaction between the steel tube and concrete core of concrete-filled steel tube columns. Bahrami *et al.* [7] examined unstiffened and stiffened concrete-filled steel composite columns. Bahrami *et al.* [8, 9] assessed axially and eccentrically loaded tapered concrete-filled steel composite columns. A nonlinear finite element model was presented by Dai *et al.* [10] to predict the behaviour of concrete-filled steel tubular columns with elliptical hollow sections under axial compression. Essopjee and Dundu [11] performed tests of concrete-filled double-skin circular tube columns subjected to axial compression until failure. Concrete-filled steel tube columns were experimentally tested by Ekmekyapar and AL-Eliwi [12] to assess the impact of columns parameters and confinement effect on their performance. The behaviour of elliptical concrete-filled columns under either concentric or eccentric compressive load was numerically studied by Qiu *et al.* [13]. Liang [14] proposed a mathematical model to compute the axial load-deflection performance of high-strength circular double-skin concrete-filled steel tubular columns subjected to eccentric loading. He *et al.* [15] evaluated the flexural buckling behaviour and resistances of circular high strength concrete-filled stainless steel tube columns based on experiments and numerical modelling. Ahmed *et al.* [16] provided computational and design models for the simulation and design of eccentrically loaded high-strength circular concrete-filled double steel tubular columns composed of circular thin-walled sections.

To avoid loss of life and damage to structures due to seismic or large lateral loads, the need for columns that can absorb the energy of the loads is essential. High energy absorbing columns are utilised to decrease the unwanted effects of seismic or large lateral loads [17]. Thus, the energy absorption capacity is an important criterion for structures that are exposed to these kinds of loads. Accordingly, the energy absorption capacity of the CFTS columns with different aspect ratios is evaluated in this paper. The finite element software ABAQUS is utilised to simulate and analyse the CFTS columns nonlinearly. After validating the simulation, the columns are developed. Various parameters such as load eccentricities, cross-sectional shapes, and steel tube thicknesses are considered for the columns with the aspect ratios of 6, 10, and 13 in order to assess their effects on the energy absorption capacity of the CFTS columns.

2. Materials and Methods

An experimental testing of a CFTS column is described here which was used for validating the simulation of the columns. Also, details of the simulation, validation method, and development of the simulated CFTS columns are presented.

2.1 Experimental test

An experimental test was conducted on a CFTS column with an aspect ratio of 10 [18]. The main geometric specifications of the tested column were diameter D as 114.3 mm and thickness of the steel tube t as 3.35 mm. The yield stress of the perimeter steel tube was 287.33 MPa, and this was a result from the performed tension tests on I specimens according to ASTM A370-07a [19]. The concrete compressive strength obtained from testing cylindrical concrete specimens with the dimensions of 10 cm \times 20 cm at 28 days was 88.8 MPa. An Instron 8506 servo hydraulic actuator with electronic displacement control was utilised to do the test of the column. The column was tested under the concentric loading on its entire section until failure. This tested column with its all specifications was considered for validating the simulation method of the columns.

2.2 Simulation, validation, and development of simulated columns

The tested CFTS column described in section 2.1 of this paper was simulated utilising the finite element software ABAQUS to validate the simulation. Materials, loading, and boundary conditions of the column were completely simulated based on the test. The boundary conditions were appropriately simulated by restraining the nodes corresponding to the support points. The pin-pin boundary conditions were adopted in the finite element model. Consequently, the rotations of the top and bottom surfaces of the column in the X, Y, and Z directions were free. Moreover, the displacements of the top and bottom surfaces in the X and Z directions were restrained. However, the displacement of the top surface in the Y direction, the direction of the applied load, was free while that of the bottom surface was restrained [20]. The main materials of the column, steel tube and concrete core, were simulated considering their features. A bilinear steel material model which included progressive hardening behaviour and softening effects was adopted for the tube [21, 22]. Figure 1 shows the steel material model. In the Figure, σ and ε were the uniaxial stress and its corresponding axial strain, respectively. When strains were larger than ε_Y , a strain increment $d\varepsilon$ included elastic and plastic contributions, respectively as $d\varepsilon^e$ and $d\varepsilon^p$.

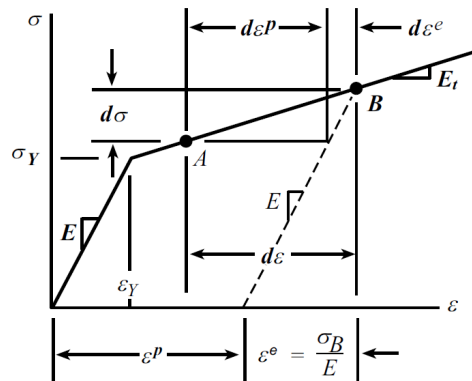


Figure 1. Steel material model [23, 24]

Concurrently, a concrete damage plasticity model was considered for the core [25]. Figure 2 illustrates the concrete material model. As it is displayed in the Figure, the total strain tensor ε consisted of the elastic and plastic parts as ε^{el} and ε^{pl} , respectively. Two scalar damage variables, d_t and d_c , were ranged from 0 (undamaged) to 1 (fully damaged). The inelastic compression strain $\varepsilon_c^{in,h}$ and the cracking strain $\varepsilon_t^{ck,h}$ represented the isotropic hardening variables and were composed of the plastic hardening strain $\varepsilon^{pl,h}$ plus the residual strain due to damages. Two hardening variables $\varepsilon_c^{pl,h}$ and $\varepsilon_t^{pl,h}$ designated the equivalent plastic strains in compression and tension, which also presented the damage states in compression and tension, respectively. Furthermore, σ_c , ε_c , and σ_{cu} were considered as the nominal compressive stress, nominal compressive strain, and ultimate compressive strength of the unconfined cylinder specimen, respectively. The tensile strength σ_{t0} is generally adopted as 7% to 10% of the ultimate compressive strength σ_{cu} , however in the present study, the maximum value as $0.1\sigma_{cu}$ was taken into account for σ_{t0} . While σ_t and ε_t were the uniaxial tensile response of concrete under tension load and its corresponding strain, respectively. The modulus of elasticity was E_0 .

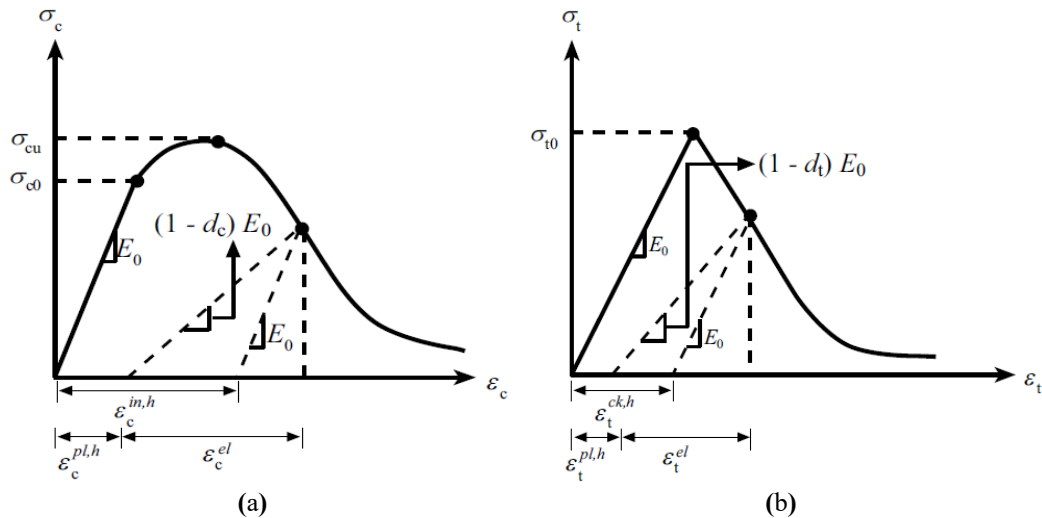


Figure 2. Concrete material model: (a) Compression, (b) Tension [26]

The Poisson's ratios of concrete and steel of the column were 0.2 and 0.3, respectively. To account for the confinement effect of the steel tube on the concrete core, the ratio of the second stress invariants on the tensile and compressive meridians (K_c) was taken as 0.667 [27-29]. The solid element C3D8R was used for the simulation of the concrete core, however, the shell element S4R was utilised for the simulation of the steel tube. The Embedded Region constraint with the friction coefficient of 0.3 was employed for the contact between the concrete core and steel tube [27-29]. The load was applied to the column using the displacement control. In order to accomplish accurate results, a suitable mesh size should be considered for the model. Thus, a convergence study was conducted on the mesh size of the model. Various mesh sizes were examined for the simulated column and finally the mesh size of 15 mm, a mesh size that would produce the most accurate result, was concluded to be the most suitable mesh size for the column.

Since the tested column was completely simulated following the pre-mentioned explanations, the obtained load-axial strain curve from the nonlinear finite element analysis was compared with that from the experimental test. This comparison is demonstrated in Figure 3. As can

be seen from the Figure, the difference between the curves was slight and their similarities clearly stated that the simulation method of this study was sufficiently valid.

Considering the validated simulation method, the column was then developed under different conditions. Aspect ratios of the columns were 6, 10, and 13. Concrete compressive strengths of 32.7 MPa and 88.8 MPa were employed for the columns. Load was applied to the columns with various eccentricities of 0 mm, 25 mm, and 50 mm. Other shapes, square and rectangular, were also used for the cross-section of the columns. Different steel tube thicknesses of 2 mm, 3.35 mm, and 5 mm were utilised for the columns. The developed columns were simulated following the validated simulation method. Accordingly, fifteen columns were simulated and analysed nonlinearly. The results of the analyses were then obtained, and they are presented and discussed in the section below.

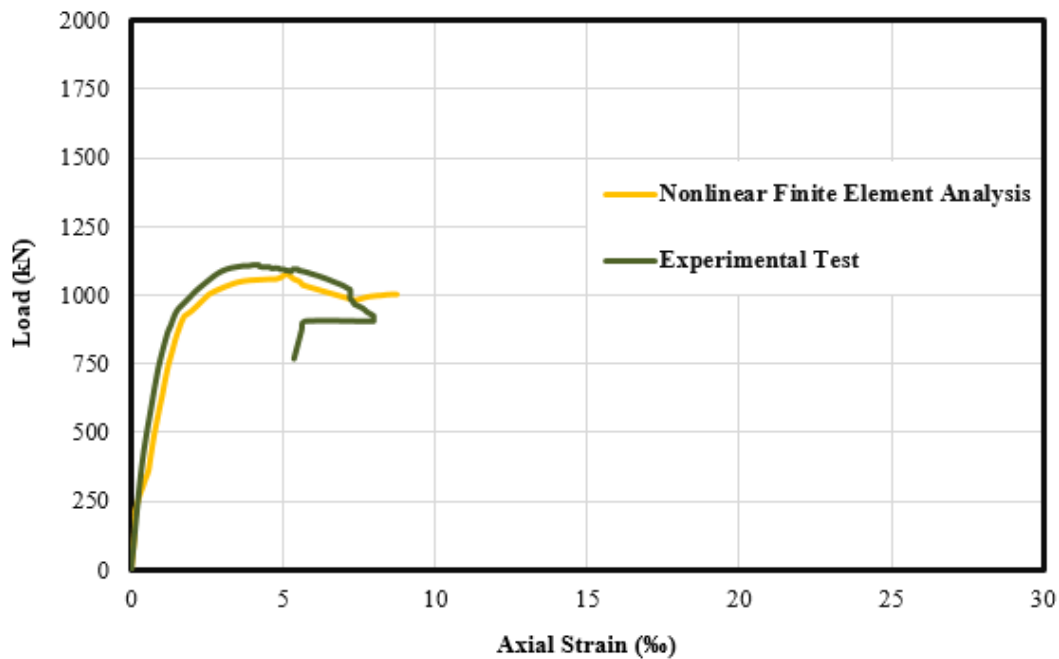


Figure 3. Validation of simulation

3. Results and Discussion

This section discusses the achieved results from the nonlinear finite element analyses of the columns under different conditions. In the following subsections, the first letter in the labels of the columns as *C*, *S*, or *R*, respectively indicates the cross-sectional shape of the columns as circular, square, or rectangular. However, the first number in the labels refers to the concrete compressive strength of the columns. Moreover, in the labels of the columns, the aspect ratios (length/diameter), L/D , of 6, 10, and 13 for the circular columns are respectively represented by 6D, 10D, and 13D, while the aspect ratio (length/width), L/B , of 10 for the rectangular and square columns is designated by 10B. The values of the load eccentricity and steel tube thickness in mm are respectively followed after e and t in the labels of the columns.

3.1 Effect of load eccentricity on energy absorption capacity of CFTS columns

The reduction of the energy absorption capacity was witnessed for the CFTS columns as their load eccentricity was increased. This issue can be observed from the diagrams in Figure 4, which uncover the effect of the load eccentricity on the energy absorption capacity of the columns with different aspect ratios of 6, 10, and 13. For example, in the case of the column with aspect ratio of 13, the energy absorption capacity of C-80-13D-e0-t3.35 was decreased from 10077 kN.mm to 3818 kN.mm (C-80-13D-e50-t3.35) when the load eccentricity was increased from 0 mm to 50 mm, implying an energy absorption capacity reduction of 62.1%. Since the steel tube played a major role in the energy absorption capacity of the columns, the main reason for the reduction of the energy absorption capacity can be pointed to the non-uniform use of the steel tube capacity owing to the existence of the eccentricity for the load, because asymmetric tensile and compressive stresses which were created by the eccentric load were intensified with the increase of the load eccentricity that concluded lower energy absorption capacity of the columns. Also, because in the columns with 0 mm eccentricity, the total cross-sectional capacity uniformly resisted the compressive forces created by the applied load, however, by deviation of the load from the centre of the columns, less cross-sectional area of the columns was affected by the same amount of the force which produced more stresses in small areas of the columns that resulted in the reduction of the energy absorption capacity of the columns.

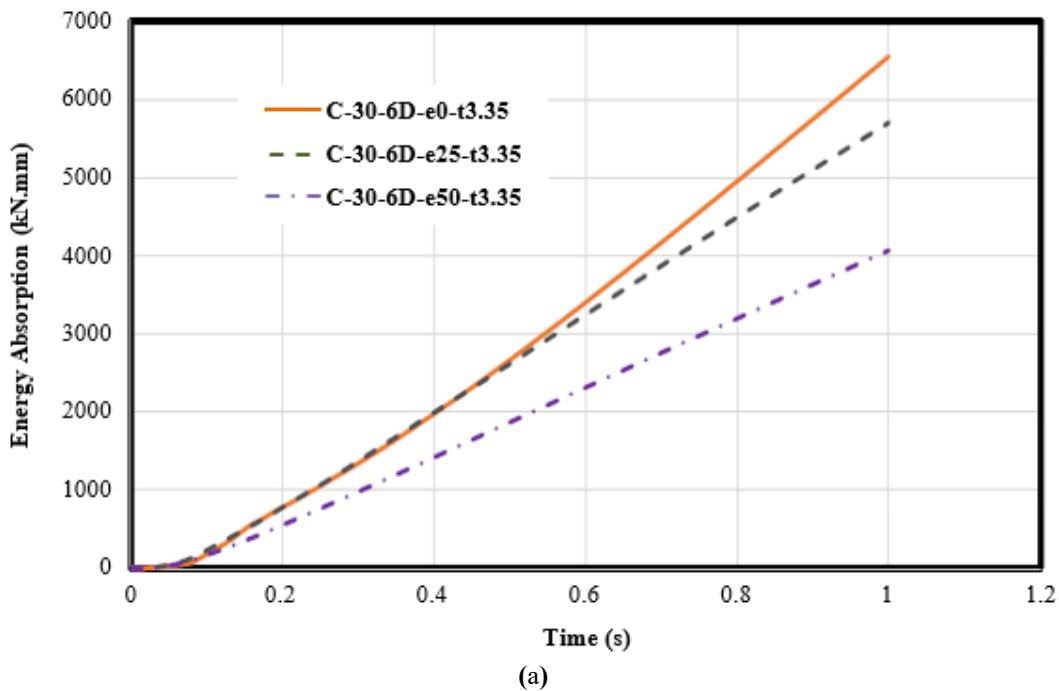
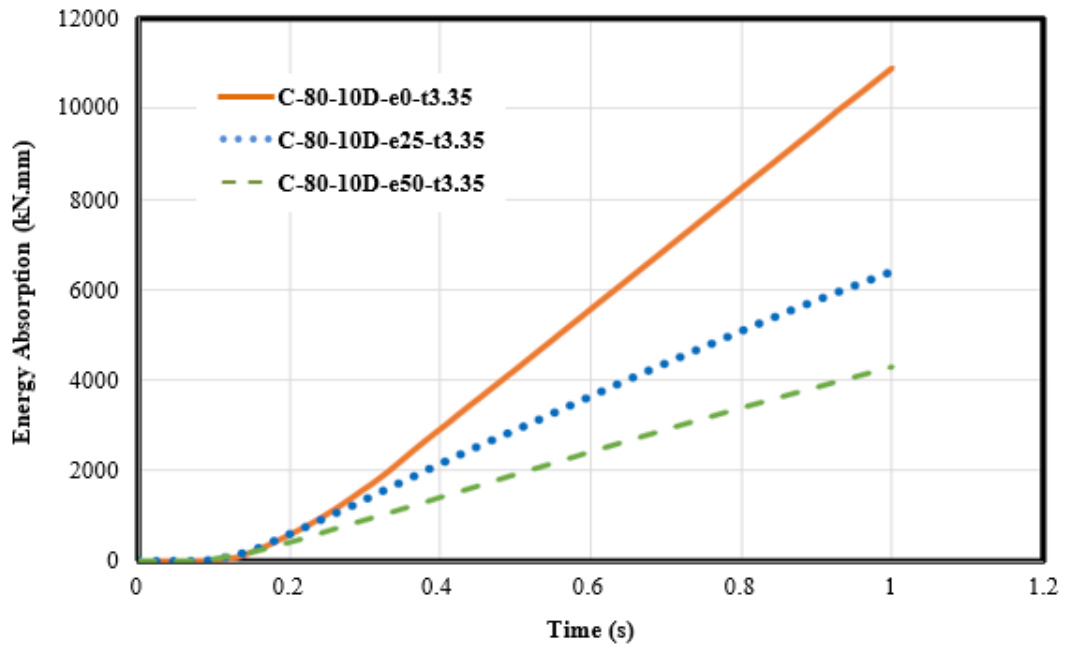
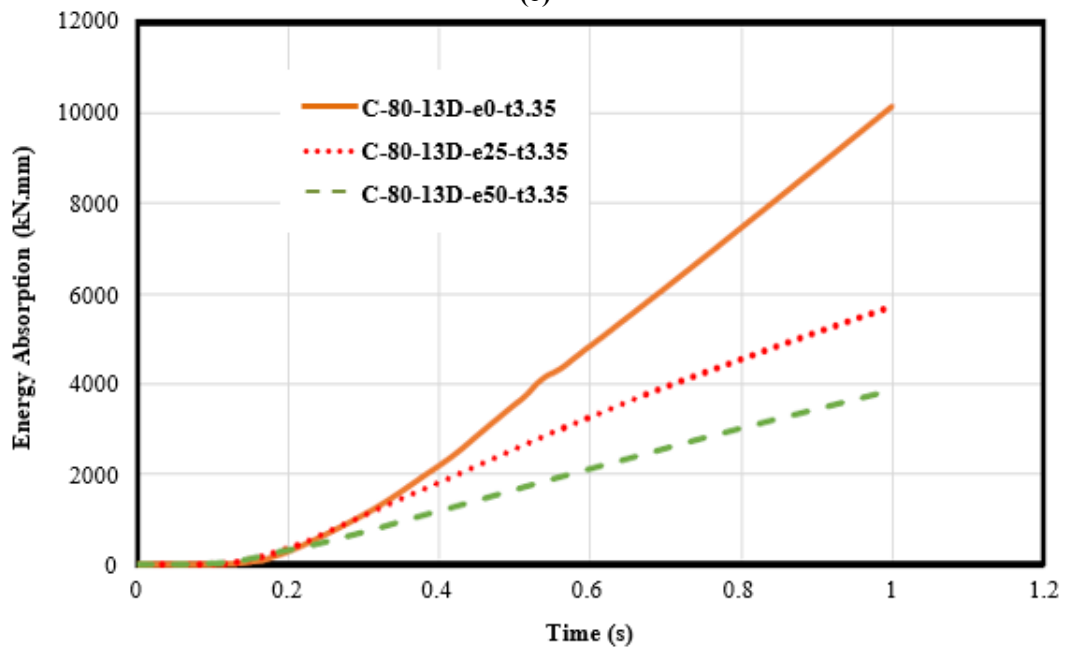


Figure 4. Effect of load eccentricity on energy absorption capacity of CFTS columns with different aspect ratios: (a) $L/D = 6$, (b) $L/D = 10$, (c) $L/D = 13$



(b)



(c)

Figure 4.

Figure 4. (Continued) Effect of load eccentricity on energy absorption capacity of CFTS columns with different aspect ratios: (a) $L/D = 6$, (b) $L/D = 10$, (c) $L/D = 13$

3.2 Effect of aspect ratio on energy absorption capacity of CFTS columns

The changes of the energy absorption capacity of the columns due to the change of their aspect ratio from 10 to 13 are displayed in Figure 5. The Figure demonstrates that the increase of the aspect ratio decreased the energy absorption capacity of the columns. As the aspect ratio was increased from 10 to 13 for the columns with various load eccentricities of 0 mm, 25 mm, and 50 mm, their energy absorption capacity was respectively reduced from 10899 kN.mm to 10077 kN.mm, from 6396 kN.mm to 5679 kN.mm, and from 4290 kN.mm to 3818 kN.mm, signifying respective reductions of 7.5%, 11.2%, and 11% in their energy absorption capacity. Enhancing the aspect ratio increased the buckling of the columns which adversely influenced their energy absorption capacity.

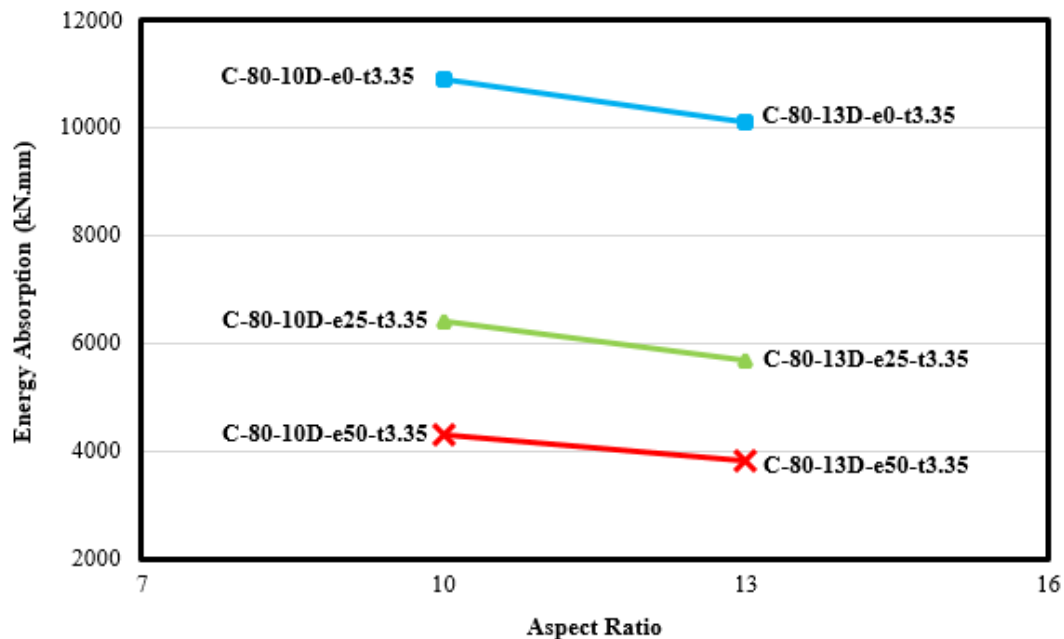


Figure 5. Effect of aspect ratio on energy absorption capacity of CFTS columns

3.3 Effect of cross-sectional shape on energy absorption capacity of CFTS columns

Figure 6 elaborates the effect of different cross-sectional shapes on the energy absorption capacity of the columns. The energy absorption capacity of the circular CFTS column was reduced by 45.6% and 48.9% as its cross-sectional shape was respectively changed to the rectangular and square shapes. This was owing to the issue that the created loop stresses by the steel tube were distributed more appropriately and uniformly in the circular column than in the square and rectangular columns, because the circular column did not have plane sides. Meanwhile, by changing the cross-section of the column from the rectangular to square shape, its energy absorption capacity was reduced by 5.9%. Therefore, the cross-sectional shapes of the circular, rectangular, and square were respectively effective on the energy absorption capacity of the CFTS columns.

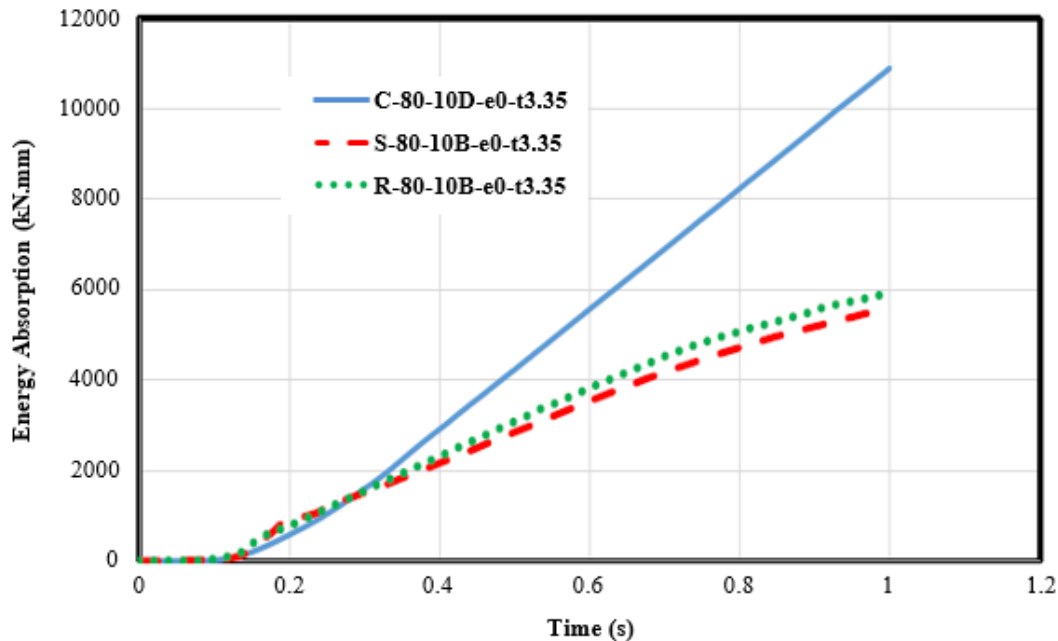


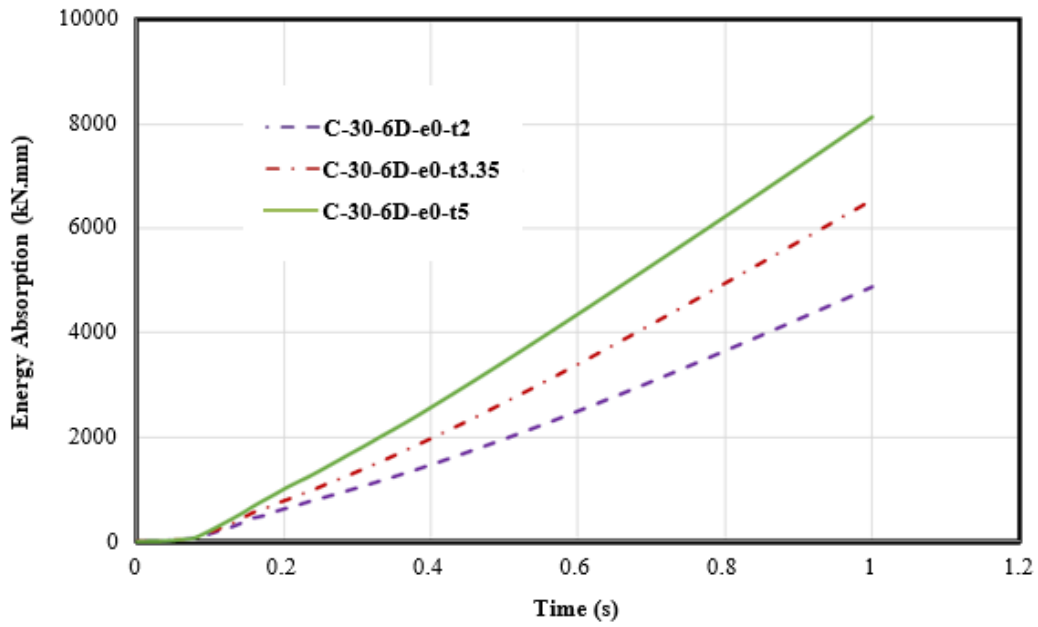
Figure 6. Effect of cross-sectional shape on energy absorption capacity of CFTS columns with aspect ratio of 10

3.4 Effect of steel tube thickness on energy absorption capacity of CFTS columns

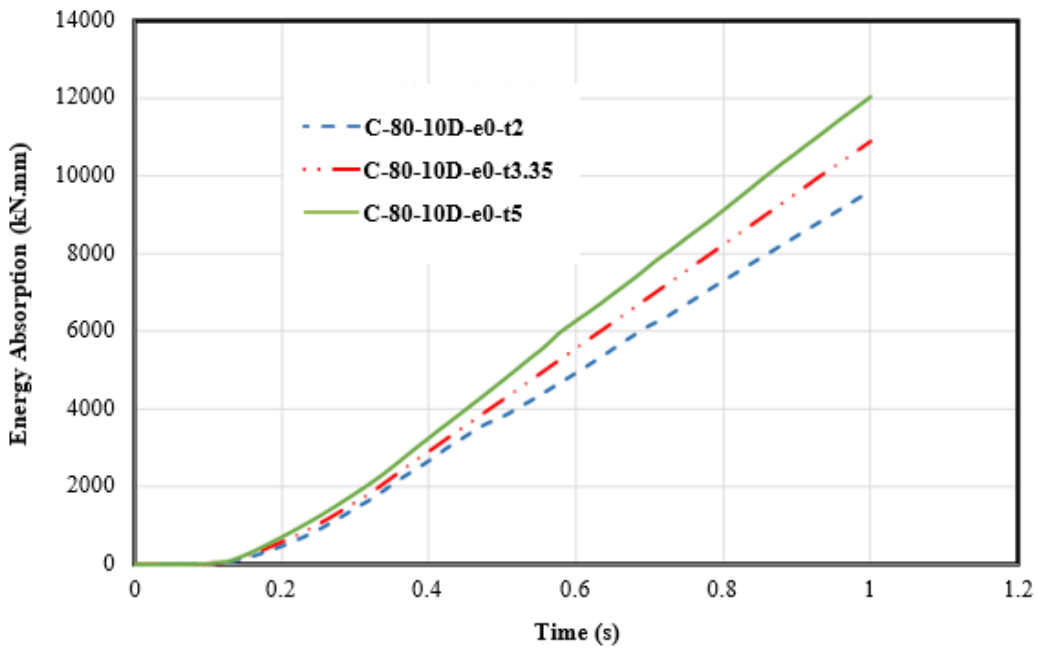
Various circular CFTS columns with different steel tube thicknesses, concrete compressive strengths, and aspect ratios were analysed under the load with 0 mm eccentricity and the resulting energy absorption capacity diagrams are presented in Figure 7. The improvement of the energy absorption capacity of the columns by the enhancement of the steel tube thickness is indicated in the Figure. For instance, the increase of the steel tube thickness from 2 mm in C-30-6D-e0-t2 to 3.35 mm in C-30-6D-e0-t3.35 and 5 mm in C-30-6D-e0-t5, resulted in the enhancement of the energy absorption capacity of the columns as 34.1% and 24.3%, respectively. It was because of the point that larger steel tube thickness caused greater confinement effect of the steel tube on the concrete core of the columns, which led to their higher energy absorption capacity.

3.5 Failure modes of CFTS columns

Figures 8 and 9 show the typical failure modes of the columns. According to Figure 8, buckling of the column with 0 mm eccentricity was less significant than that of the columns with the eccentricities of 25 mm and 50 mm. Larger buckling of the columns loaded with larger eccentricities led to their lower energy absorption capacity, which was also noticed in section 3.1. Buckling of the eccentrically loaded columns occurred close to their top. Moreover, local buckling was observed for the failed columns with different steel tube thicknesses, as demonstrated in Figure 9.



(a)



(b)

Figure 7. Effect of steel tube thickness on energy absorption capacity of CFTS columns with different aspect ratios: (a) $L/D = 6$, (b) $L/D = 10$, (c) $L/D = 13$

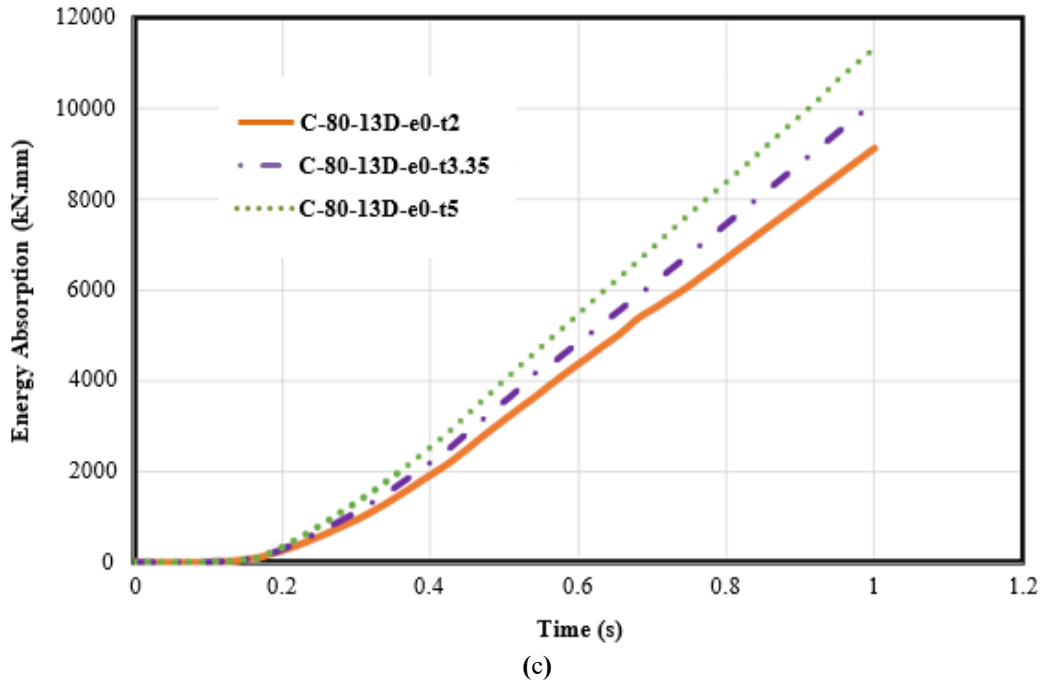


Figure 7. (Continued) Effect of steel tube thickness on energy absorption capacity of CFTS columns with different aspect ratios: (a) $L/D = 6$, (b) $L/D = 10$, (c) $L/D = 13$

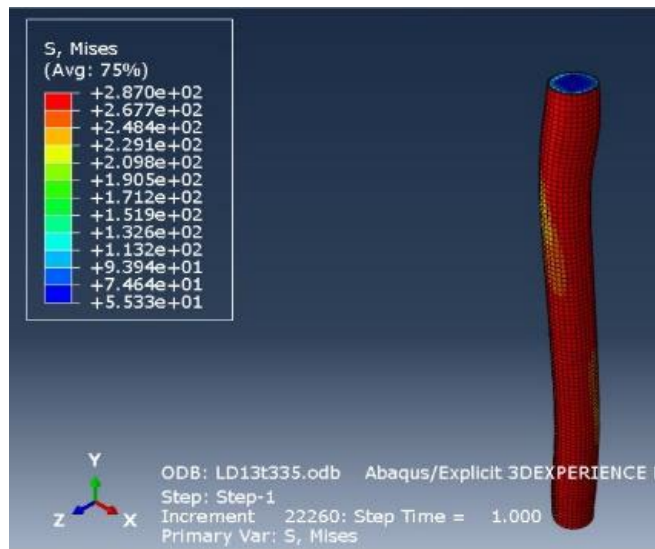
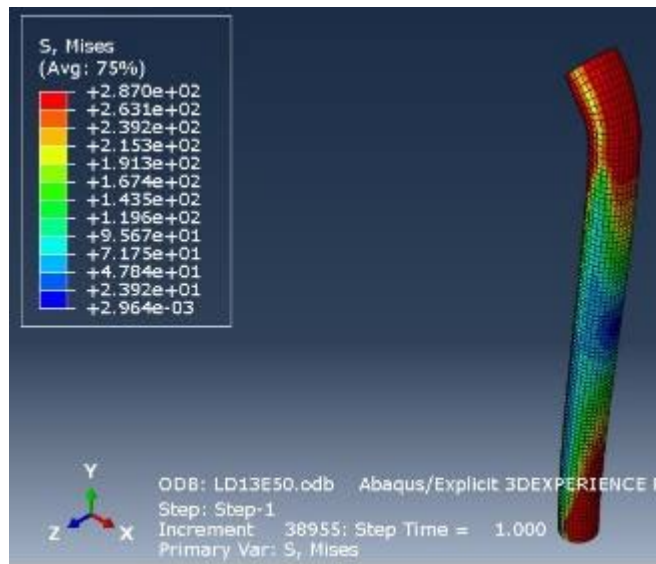
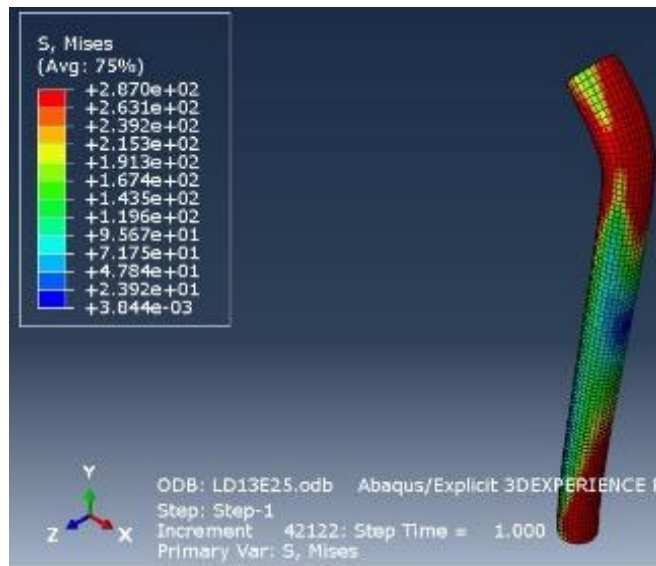


Figure 8. Typical failure modes of CFTS columns under different load eccentricities: (a) C-80-13D-e0-t3.35, (b) C-80-13D-e25-t3.35, (c) C-80-13D-e50-t3.35

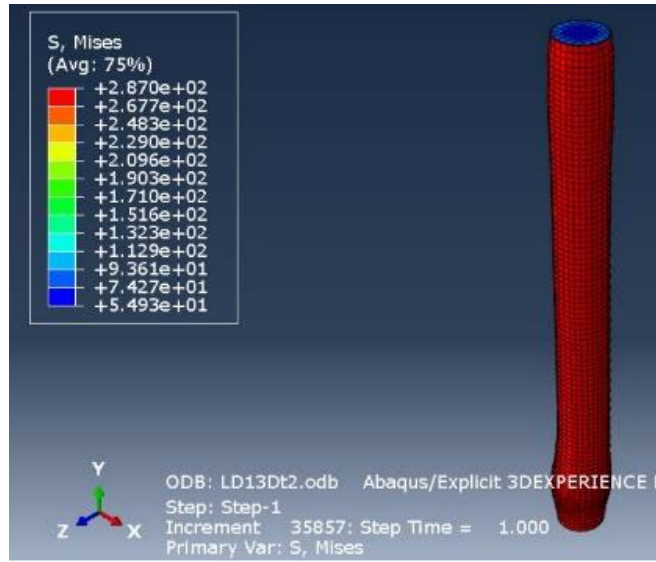


(b)

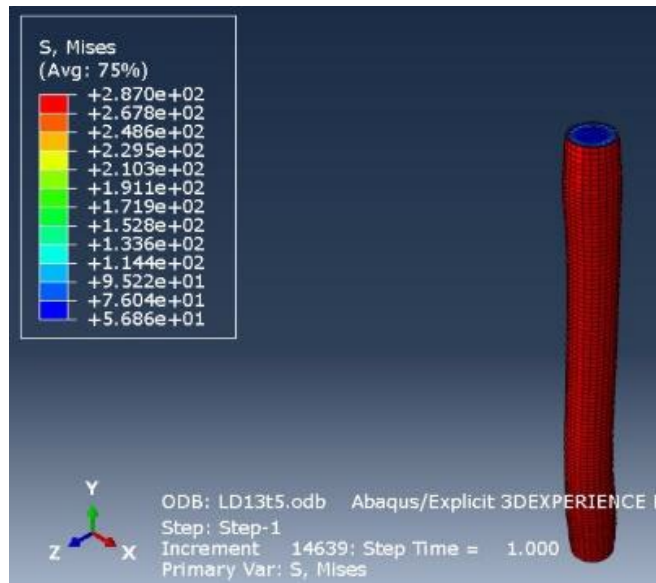


(c)

Figure 8. (Continued) Typical failure modes of CFTS columns under different load eccentricities:
(a) C-80-13D-e0-t3.35, (b) C-80-13D-e25-t3.35, (c) C-80-13D-e50-t3.35



(a)



(b)

Figure 9. Typical failure modes of CFTS columns with different steel tube thicknesses: (a) C-80-13D-e0-t2, (b) C-80-13D-e0-t5

4. Conclusions

The CFTS columns with different aspect ratios were analysed to assess their energy absorption capacity. The simulation and analysis of the columns were done by the use of the finite element software ABAQUS. Comparing the results achieved from the finite element analysis of the CFTS column and its experimental test validated the simulation of the columns. Then, the columns were developed. The energy absorption capacity of the columns was evaluated and discussed under different conditions including various load eccentricities, cross-sectional shapes, and steel tube thicknesses. It was revealed that the enhancement of the load eccentricity or aspect ratio resulted in the reduction of the energy absorption capacity of the CFTS columns. Therefore, the applied load with 0 mm eccentricity and lowest aspect ratio ($L/D = 6$) were preferred for the columns, from an energy absorption capacity perspective. The circular column displayed greater energy absorption capacity than the rectangular and square columns. The energy absorption capacity of the CFTS columns was improved as the steel tube thickness was increased. Buckling was the dominant failure mode of the columns, and a higher degree of buckling occurred in the columns with larger eccentricities.

References

- [1] Uy, B., 1998. Ductility, strength and stability of concrete-filled fabricated steel box columns for tall buildings. *The Structural Design of Tall and Special Buildings*, 7(2), 113-133.
- [2] Han, L.H. and Yao, G.H., 2003. Behaviour of concrete-filled hollow structural steel (HSS) columns with preload on the steel tubes. *Journal of Constructional Steel Research*, 59(12), 1455-1475.
- [3] Ellobody, E. and Young, B., 2006. Design and behaviour of concrete-filled cold-formed stainless steel tube columns. *Engineering Structures*, 28(5), 716-728.
- [4] Lam, D. and Gardner, L., 2008. Structural design of stainless steel concrete filled columns. *Journal of Constructional Steel Research*, 64(11), 1275-1282.
- [5] Yang, Y.F. and Han, L.H., 2009. Experiments on rectangular concrete-filled steel tubes loaded axially on a partially stressed cross-sectional area. *Journal of Constructional Steel Research*, 65(8-9), 1617-1630.
- [6] Starossek, U., Falah, N. and Lohning, T., 2010. Numerical analyses of the force transfer in concrete-filled steel tube columns. *Structural Engineering and Mechanics*, 35(2), 241-256.
- [7] Bahrami, A., Wan Badaruzzaman, W.H. and Osman, S.A., 2011. Nonlinear analysis of concrete-filled steel composite columns subjected to axial loading. *Structural Engineering and Mechanics*, 39(3), 383-398.
- [8] Bahrami, A., Wan Badaruzzaman, W.H. and Osman, S.A., 2012. Structural behaviour of tapered concrete-filled steel composite (TCFSC) columns subjected to eccentric loading. *Computers and Concrete*, 9(6), 403-426.
- [9] Bahrami, A., Wan Badaruzzaman, W.H. and Osman, S.A., 2013. Performance of axially loaded tapered concrete-filled steel composite slender columns. *Journal of Civil Engineering and Management*, 19(5), 705-717.
- [10] Dai, X.H., Lam, D., Jamaluddin, N. and Ye, J., 2014. Numerical analysis of slender elliptical concrete filled columns under axial compression. *Thin-Walled Structures*, 77, 26-35.
- [11] Essopjee, Y. and Dundu, M., 2015. Performance of concrete-filled double-skin circular tubes in compression. *Composite Structures*, 133, 1276-1283.
- [12] Ekmekyapar, T. and AL-Eliwi, B.J.M., 2016. Experimental behavior of circular concrete filled steel tube columns and design specifications. *Thin-Walled Structures*, 105, 220-230.

- [13] Qiu, W., McCann, F., Espinos, A., Romero, M.L. and Gardner, L., 2017. Numerical analysis and design of slender concrete-filled elliptical hollow section columns and beam-columns. *Engineering Structures*, 131, 90-100.
- [14] Liang, Q.Q., 2018. Numerical simulation of high strength circular double-skin concrete-filled steel tubular slender columns. *Engineering Structures*, 168, 205-217.
- [15] He, A., Liang, Y. and Zhao, O., 2020. Flexural buckling behaviour and resistances of circular high strength concrete-filled stainless steel tube columns. *Engineering Structures*, 219, 110893, <https://doi.org/10.1016/j.engstruct.2020.110893>.
- [16] Ahmed, M., Liang, Q.Q., Patel, V.I. and Hadi, M.N.S., 2020. Computational simulation of eccentrically loaded circular thin-walled concrete-filled double steel tubular slender columns. *Engineering Structures*, 213, 110571, <https://doi.org/10.1016/j.engstruct.2020.110571>.
- [17] Alavi Nia, A. and Parsapour, M., 2014. Comparative analysis of energy absorption capacity of simple and multi-cell thin-walled tubes with triangular, square, hexagonal and octagonal sections. *Thin-Walled Structures*, 74, 155-165.
- [18] Oliveira, W.L.A., De Nardin, S., El Debs, A.L.H.C. and El Debs, M.K., 2009. Influence of concrete strength and length/diameter on the axial capacity of CFT columns. *Journal of Constructional Steel Research*, 65(12), 2103-2110.
- [19] ASTM A370-07a., 2007. *Standard Test Methods and Definitions for Mechanical Testing of Steel Products*. West Conshohocken: ASTM International.
- [20] Bahrami, A., Wan Badaruzzaman, W.H. and Osman., S.A., 2013. Investigation of concrete-filled steel composite (CFSC) stub columns with bar stiffeners, *Journal of Civil Engineering and Management*, 19(3), 433-446.
- [21] Bahrami, A. and Yavari, M., 2019. Performance of steel-concrete shear walls with two-sided reinforced concrete. *International Journal of Engineering and Technology Innovation*, 9(3), 228-239.
- [22] Bahrami, A. and Matinrad, S., 2019. Response of steel beam-to-column bolted connections to blast loading. *International Journal of Recent Technology and Engineering*, 8(3), 3639-3648.
- [23] Cook, R.D., Malkus, D.S., Plesha, M.E. and Witt, R.J., 2002. *Concepts and Applications of Finite Element Analysis*. 4th ed. New York: John Wiley & Sons.
- [24] Wester, M., 2004. *Finite Element Modelling of Mast Foundation and T-Joint*. Stockholm: Royal Institute of Technology.
- [25] Bahrami, A. and Yavari, M., 2019. Hysteretic assessment of steel-concrete composite shear walls. *International Journal of Recent Technology and Engineering*, 8(2), 5640-5645.
- [26] Hafezolzghorani, M., Hejazi, F., Vaghei, R., Jaafar, M.S. and Karimzade, K., 2017. Simplified damage plasticity model for concrete. *Structural Engineering International*, 27(1), 68-78.
- [27] Qiu, W., McCann, F., Espinos, A., Romero, M.L. and Gardner, L., 2017. Numerical analysis and design of slender concrete-filled elliptical hollow section columns and beam-columns. *Engineering Structures*, 131, 90-100.
- [28] Bahrami, A. and Mahmoudi Kouhi, A., 2020. Compressive behaviour of circular, square, and rectangular concrete-filled steel tube stub columns. *Civil Engineering and Architecture*, 8(5), 1119-1126.
- [29] Wang, C., Yun, Z., Kang, J., Zhou, Y., Chen, M. and Wu, Y., 2019. Behavior of an innovative square composite column made of four steel tubes at the corners and corrugated steel batten plates on all sides. *Advances in Civil Engineering*, 2971962, <https://doi.org/10.1155/2019/2971962>.